JOURNAL OF MAGNETIC RESONANCE **125,** 376–382 (1997)
ARTICLE NO. MN971139

Amplitude-Modulated Decoupling Pulses in Liquid-State NMR

HELEN GEEN* AND JEAN-MARC BÖHLEN†

*Department of Physics, University of Nottingham, University Park, Nottingham, NG7 2RD, United Kingdom; and †Spectrospin AG, Faellenden, Switzerland

Received December 11, 1996; revised January 24, 1997

Considerable attention over the years has focused on the development of techniques for heteronuclear spin decoupling in liquid-state NMR experiments. The quest for broadband methods has taken particular priority, driven by the need to decouple over an ever increasing range of chemical shifts of the heteronucleus with an economical use of power (*1–14*). The routine approach involves the repetitive application of a cyclic irradiation sequence which is composed of a number of discrete, inherently broadband inversion pulses arranged to effect no overall rotation of the spin magnetization. Originally, such cycles used composite inversion pulses (*15*) of the kind which form the MLEV (*1, 2*), WALTZ (*5*), and GARP (*6*) sequences. More recently, cyclic combinations of continuously modulated inversion pulses have been devised (*9–14*), and found among these are some of the broadest bandwidth methods seen to date. Modulated selective-inversion pulses have also been incorporated into the same framework with the different aim of decoupling over only a narrow range of chemical shifts without affecting the remainder of the spectrum (*16–19*).

Central to the work presented here is a novel kind of decoupling scheme which uses a single, inherently cyclic, amplitude-modulated pulse in place of the train of inversion pulses used more routinely (*20*). The shaped pulse, which spans a full period of the decoupling irradiation, has an amplitude profile described by a simple Fourier series. The amplitude variations are thus smooth and continuous throughout the entire decoupling process. To satisfy the theoretical criteria for good decoupling (*3, 4, 7*), the Fourier coefficients are tailored to give a pulse which is broadband and cyclic, meaning here that the propagator equals the equal identity matrix over a wide range of resonance offsets relative to the RMS pulse amplitude. Because of the small number of Fourier harmonics present in the decoupling irradiation, the response of the observed nucleus shows resonances outside the decoupled frequency band typical of fully coupled spins. The method can thus be said to be band-selective (*21*) as well as broadband, suggesting a use in experiments which call for low-power decoupling over a prescribed frequency range of wide extent with no apparent perturbation elsewhere in the spectrum.

The theoretical scheme used for designing the amplitude modulations was described earlier (*20*). It is based on the use of the Floquet formalism (*22–27*), due originally to Shirley (*22*), with which a periodic time-dependent Hilbert space Hamiltonian is transformed into a time-independent Floquet matrix $\mathcal{H}_F$ of infinite dimensionality. The Hamiltonian under consideration describes a single spin-$\frac{1}{2}$ under the action of the pulse applied at an offset ω from the resonance. To accomplish the necessary transformation to Floquet space, the amplitude modulation is written as a Fourier series of N components

$$\omega_{RF}(t) = \sum_{n=-N}^{+N} \omega_{RF}^{(n)} \exp(in\omega_\tau t) \qquad [1]$$

with a fundamental frequency

$$\omega_\tau = \frac{2\pi}{\tau} \qquad [2]$$

related to the duration τ of the pulse. The Fourier amplitudes of order n and $-n$ are disposed symmetrically such that $\omega_{RF}^{(n)} = \omega_{RF}^{(-n)*}$ and $\omega_{RF}^{(0)}$ is real. The resulting manifold of Floquet states $|\alpha, n\rangle$ and $|\beta, n\rangle$ is derived from the original spin states $|\alpha\rangle$ and $|\beta\rangle$ which are said to have been ''dressed'' with the ''photon number'' n. Such a level structure is highly periodic and each pair of the energy eigenvalues $\langle \alpha, n|\mathcal{H}_F^D|\alpha, n\rangle$ and $\langle \beta, n|\mathcal{H}_F^D|\beta, n\rangle$ (where $\mathcal{H}_F^D$ is diagonal) can be simply derived from

$$\begin{aligned} \langle \alpha, n|\mathcal{H}_F^D|\alpha, n\rangle &= \omega_\alpha + n\omega_\tau \\ \langle \beta, n|\mathcal{H}_F^D|\beta, n\rangle &= \omega_\beta + n\omega_\tau. \end{aligned} \qquad [3]$$

The values of ω_α and ω_β are the eigenvalues for the $n = 0$ states

$$\begin{aligned} \omega_\alpha &= \langle \alpha, 0|\mathcal{H}_F^D|\alpha, 0\rangle \\ \omega_\beta &= \langle \beta, 0|\mathcal{H}_F^D|\beta, 0\rangle \end{aligned} \qquad [4]$$

1090-7807/97 $25.00

and are thus referred to here as the *fundamental eigenvalues* of the system.

Related work by Vega and co-workers (*24, 25*) shows how the overall angle of rotation θ of such a pulse can be determined from the energy eigenvalues of the Floquet Hamiltonian. Indeed, as expected, only the fundamental eigenvalues ω_α and ω_β are relevant to the average rotation rate and θ can be found directly from the frequency separation

$$\theta = (\omega_\alpha - \omega_\beta)\tau. \quad [5]$$

Because of the complexity of the Floquet Hamiltonian at an arbitrary resonance offset, numerical diagonalization procedures are normally required to compute ω_α and ω_β. Exactly on resonance, however, the values can be found by inspection of the form of the matrix (*23–27*). The resulting energy separation

$$\omega_\alpha - \omega_\beta = \omega_{\mathrm{RF}}^{(0)} \text{ for } \omega = 0 \quad [6]$$

indicates that the nominal ($\omega = 0$) value θ_0 of the flip angle is controlled by the zeroth-order Fourier component

$$\theta_0 = \omega_{\mathrm{RF}}^{(0)}\tau. \quad [7]$$

The required condition of cyclicity can therefore be imposed readily at the exact resonance by omitting the constant contribution to the amplitude modulation and thus ensuring that

$$\omega_{\mathrm{RF}}^{(0)} = 0 \quad \theta_0 = 0. \quad [8]$$

Off resonance, there are inevitable departures from cyclicity because the eigenstates of the Floquet Hamiltonian are perturbed. At sufficiently small offsets $\omega \ll \omega_\tau$, the deviations in θ from the nominal value can be estimated using perturbation theory in the form originally due to Salwen (*28*). This shows that the pulse amplitude and the offset field are coupled such that

$$\theta = \theta_0 + \kappa_1|\omega|\tau + \kappa_2\omega_\tau^{-1}\omega^2\tau + \kappa_3\omega_\tau^{-2}|\omega^3|\tau + \ldots, \quad [9]$$

where the κ_n are functions of the Fourier coefficients. It can thus be seen that by judiciously shaping the pulse according to

$$\omega_{\mathrm{RF}}^{(0)} = 0 \quad \kappa_n \approx 0 \quad (n = 1, 2 \ldots) \quad [10]$$

the cyclicity of the propagator can be restored away from the resonance and the bandwidth of the decoupling can be improved.

In the first instance, pulse shapes were configured using up to five Fourier coefficients ($N \leqslant 5$) by searching for solutions to the simultaneous equations [10] and taking only the first two terms of the power series, κ_1 and κ_2, into consideration. As expected, such modulations conferred cyclicity over a relatively narrow range of offsets. The operating bandwidth of the best $N = 5$ solution found in this fashion was then broadened further by adding a second series of five higher-order Fourier harmonics at the frequencies $7\omega_\tau$, $8\omega_\tau$, $9\omega_\tau$, $10\omega_\tau$, and $11\omega_\tau$. The amplitudes of this second series of Fourier coefficients were intuitively chosen to match the original five. The resulting $N = 11$ pulse shape provided an excellent starting condition for numerical optimization which was required to raise the quality of the decoupling to a more useful level, and thus two acceptable modulations with $N = 11$ and $N = 12$ harmonics were obtained. Finally, a third acceptable $N = 17$ modulation of even broader bandwidth was similarly found by optimizing the quality of a $N = 17$ starting modulation formed by twice superimposing the same combination of five Fourier amplitudes onto the original $N = 5$ modulation, first at the frequencies $7\omega_\tau$, $8\omega_\tau$, $9\omega_\tau$, $10\omega_\tau$, and $11\omega_\tau$ as before and again at the frequencies $13\omega_\tau$, $14\omega_\tau$, $15\omega_\tau$, $16\omega_\tau$, and $17\omega_\tau$. Apparently, no further improvements to the decoupling bandwidth could be made in this way without significantly impairing the decoupling quality. The three modulations chosen for implementation are referred to here as the SWIRL (*s*haped, *wi*deband-*r*esponse, *l*ow-power) decoupling pulses.

Throughout the search, the quality of the decoupling was evaluated numerically by calculating the degree of *J* scaling attained over a range of decoupler offsets and considering the level of RF power deposition. The *J* scaling was measured as usual in terms of the parameter $\lambda = J^*/J$, where J^* is the value of the scalar interaction observed with decoupling and λ is defined formally as the first derivative of the pulse rotation angle (*3, 4, 7*)

$$\lambda = \frac{1}{\tau}\frac{\partial\theta}{\partial\omega} \quad [11]$$

and can therefore be obtained directly from the fundamental eigenvalues of the Floquet Hamiltonian (Eq. [5]). To account for the average RF power deposited during the decoupling, the offsets were measured using the ratio $\bar{\Omega} = \omega/\omega_{\mathrm{RMS}}$ where ω_{RMS} is the RMS pulse amplitude

$$\omega_{\mathrm{RMS}}^2 = \frac{1}{\tau}\int_{t=0}^{\tau}\omega_{\mathrm{RF}}(t)^2 = \omega_{\mathrm{RF}}^{(0)^2} + 2\sum_{n=1}^{N}\omega_{\mathrm{RF}}^{(n)^2}. \quad [12]$$

The numerical manipulations of the Floquet Hamiltonian required for the evaluation were performed using a suitably equipped version of the GAMMA program (*29*) together with the CERN routine MINUIT for the final optimization.

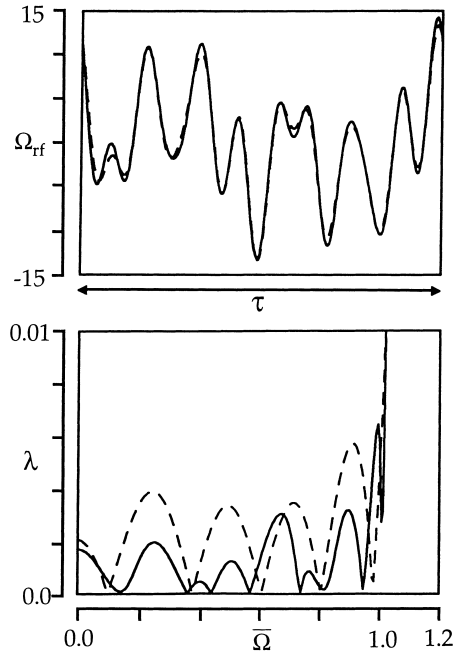

FIG. 1. Simulated waveforms and performance of the amplitude-modulated decoupling pulses SWIRL-11 (dashed lines) and SWIRL-12 (solid lines). (Upper) The modulation functions which are described by the Fourier coefficients of Table 1. (Lower) The dependence of the corresponding scaling factors on the frequency offset which is measured relative to the RMS amplitude of the pulses. Note that good decoupling is attained over an absolute offset range equal to the RMS pulse field.

Shown in Figs. 1 and 2 are the normalized pulse amplitudes $\Omega_{RF}(t) = \omega_{RF}(t)/\omega_\tau$ and the calculated scaling factors $\lambda(\bar{\Omega})$ for the three numerically refined modulations SWIRL-11 and SWIRL-12 which have $N = 11$ and $N = 12$ harmonics (Fig. 1) and SWIRL-17 which has $N = 17$ harmonics (Fig. 2). The normalized Fourier coefficients describing the shapes are contained in Tables 1 and 2. These are listed first in terms of the normalized magnitudes $|\Omega_{RF}^{(n)}| = |\omega_{RF}^{(n)}|/\omega_\tau$ and phases $\Phi^{(n)} = \arg(\Omega_{RF}^{(n)})$ of the complex coefficients defined in Eq. [1] and used above, and second in terms of the more familiar normalized sine and cosine coefficients (*21*) $A^{(n)}$ and $B^{(n)}$ of the modulation, defined by

$$\Omega_{RF}(t) = A_0 + \sum_{n=1}^{+N} [A^{(n)}\cos(n\omega_\tau t) + B^{(n)}\sin(n\omega_\tau t)], \quad [13]$$

where

$$A_0 = \Omega_{RF}^{(0)}$$
$$A^{(n)} = 2|\Omega_{RF}^{(n)}|\cos\Phi^{(n)}$$
$$B^{(n)} = -2|\Omega_{RF}^{(n)}|\sin\Phi^{(n)}. \quad [14]$$

The normalized RMS and peak values of the pulse amplitude $\Omega_{RMS} = \omega_{RMS}/\omega_\tau$ and $\Omega_{peak} = \omega_{peak}/\omega_\tau$ are also provided as these are required to calibrate the field strength and duration of the pulses experimentally so that optimal quality decoupling is obtained over the required frequency bandwidth. Details of the calibration procedure are found below. As can be seen from the scaling factor profiles of Fig. 1, the SWIRL-11 and SWIRL-12 pulses are predicted to confer high-quality decoupling ($\lambda < 0.006$) over an offset range spanning $\bar{\Omega} \approx 1$, or $\bar{\omega} \approx \omega_{RMS}$ frequency units, on either side of the resonance. The more broadband SWIRL-17 modulation is shown in Fig. 2. In this case, high-quality decoupling ($\lambda < 0.02$) is predicted over an enlarged bandwidth of $\bar{\Omega} \approx 1.75$, corresponding to an absolute frequency range of $\bar{\omega} \approx 1.75\omega_{rms}$.

In a series of experimental tests performed on a Bruker DRX system operating at a proton frequency of 600 MHz, the three SWIRL pulses of Figs. 1 and 2 were used to decouple the carbon-13 nuclei from the protons in a sample of 10 m*M* $2-^{13}$C sodium acetate enriched to 100% ($^*CH_3CO_2Na$). The results are summarized in Figs. 3 to 5.

Figure 3 shows the decoupling profile of the SWIRL waveforms (upper three traces) and also that of the composite-pulse scheme GARP (lowest trace). The measurements were made by acquiring a series of proton spectra for which the decoupler was applied at an array of offsets spanning a 30 kHz range. All four experiments were carried out at the

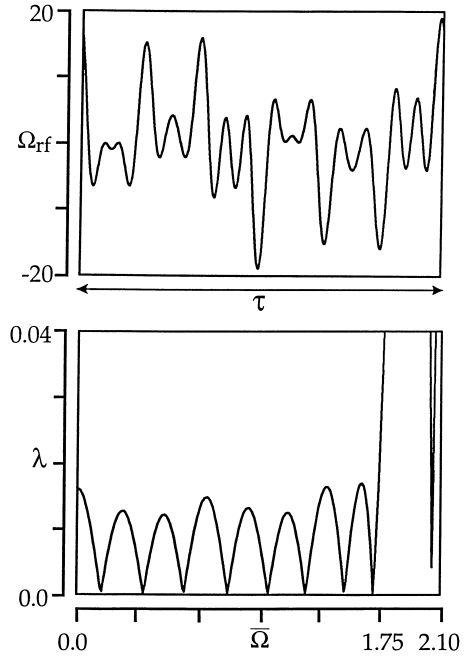

FIG. 2. Simulated waveform and performance of the amplitude-modulated decoupling pulse SWIRL-17. (Upper) The modulation function which is described by the Fourier coefficients of Table 2. (Lower) The dependence of the scaling factor on the frequency offset which is measured relative to the RMS amplitude of the pulse. Note that good decoupling is attained over an absolute offset range 75% greater than the RMS pulse field.

TABLE 1
Fourier Coefficients for the RF Modulations of Fig. 1.

	$n = 1$	$n = 2$	$n = 3$	$n = 4$	$n = 5$	$n = 6$	$n = 7$	$n = 8$	$n = 9$	$n = 10$	$n = 11$	$n = 12$	Ω_{RMS}	Ω_{peak}
$N = 11$														
$\lvert\Omega_{RF}^{(n)}\rvert$	1.58		1.70		1.90		1.86		1.81		1.25		5.88	13.33
$\Phi^{(n)}$ (rad)	−1.00		0.99		1.01		−0.94		0.99		0.97			
$A^{(n)}$	1.71		1.87		2.02		2.19		1.99		1.41			
$B^{(n)}$	2.66		−2.84		−3.22		3.00		−3.03		−2.06			
$N = 12$														
$\lvert\Omega_{RF}^{(n)}\rvert$	1.61	0.01	1.68	0.01	1.95	0.02	1.76	0.05	2.04	0.01	1.41	0.22	6.09	14.19
$\Phi(n)$ (rad)	−1.01	−1.86	0.99	−2.16	1.04	1.30	−1.03	1.10	1.06	−2.11	1.04	1.32		
$A^{(n)}$	1.71	−0.01	1.84	−0.01	1.97	0.01	1.81	0.05	1.99	−0.01	1.43	0.11		
$B^{(n)}$	2.73	0.02	−2.81	0.02	−3.36	−0.04	3.02	−0.09	−3.56	0.02	−2.43	−0.43		

Note. $\Omega_{RF}^{(0)} = 0$.

same average power level. For the three SWIRL modulations, the durations and peak RF fields of the pulses were calibrated to give an RMS amplitude of $\omega_{RMS}/2\pi = 1.5$ kHz while for the GARP sequence, a constant RF field of 1.5 kHz was used. It can be seen from the results that, at this power level, each SWIRL waveform decouples well over the predicted frequency bandwidth of $\pm\varpi/2\pi = \pm\omega_{RMS}/2\pi = \pm 1.5$ kHz for the SWIRL-11 and SWIRL-12 pulses and $\varpi/2\pi = \pm 1.75\omega_{RMS}/2\pi = \pm 2.6$ kHz for SWIRL-17.

Evident from Fig. 3 is the fact that the SWIRL waveforms are both broadband in the sense that high-quality, uniform decoupling is obtained over a wide range of offsets per unit RF power, and band selective with respect to the overall shape of the decoupling profile. The broadband behavior of the SWIRL pulses can be seen to be comparable to that of routinely used composite-pulse schemes. Indeed, the operating bandwidth of SWIRL-17 is approaching that of GARP. However, band selectivity appears to be a property associated uniquely with modulations of the SWIRL variety. In each SWIRL experiment, it can be seen that while good decoupling is maintained up to the limits of the predicted bandwidth, the responses outside the operating region show fully coupled resonances largely unperturbed by the decoupling irradiation. SWIRL decoupling is thus expected to be of considerable use in experiments which call for a low-power decoupling scheme that performs well over a selected broad region of the spectrum and leaves the remainder of the spectrum unperturbed. In contrast, the GARP sequence causes significant perturbation of the unselected resonances. Similar behavior is expected to be typical of all decoupling schemes based on composite cycles and precludes the use of such methods in experiments where a degree of selectivity is required. It is presumed that the band-selective effect of the continuous SWIRL modulations can be attributed to the compact range of the frequency components imposed on the decoupler irradiation by the simple Fourier modulation chosen at the outset.

As important as the degree of J scaling attained by a decoupling scheme is the degree to which cycling sideband resonances are excited in the observed spectrum. Undesirable resonances of this kind are usually most apparent in low-power applications of decoupling for which the period of cycling of the schemes become prohibitively long. To assess the extent of the sideband problem associated with the SWIRL pulses, a set of three experiments using the different RMS pulse fields of 300 Hz, 1.5 kHz, and 4.17 kHz

TABLE 2
Fourier Coefficients for the RF Modulations of Fig. 2

	$n = 1$	$n = 3$	$n = 5$	$n = 7$	$n = 9$	$n = 11$	$n = 13$	$n = 15$	$n = 17$	Ω_{RMS}	Ω_{peak}
$N = 17$											
$\lvert\Omega_{RF}^{(n)}\rvert$	1.48	1.59	1.62	1.49	1.58	1.82	2.05	1.87	1.36	7.06	18.91
$\Phi(n)$ (rad)	−0.96	0.98	1.00	−1.00	1.00	1.03	−0.93	0.92	1.16		
$A^{(n)}$	1.70	1.77	1.75	1.61	1.71	1.87	2.45	2.27	1.09		
$B^{(n)}$	2.42	−2.64	−2.73	2.51	−2.66	−3.12	3.29	−2.98	−2.49		

Note. $\Omega_{RF}^{(0)} = 0$.

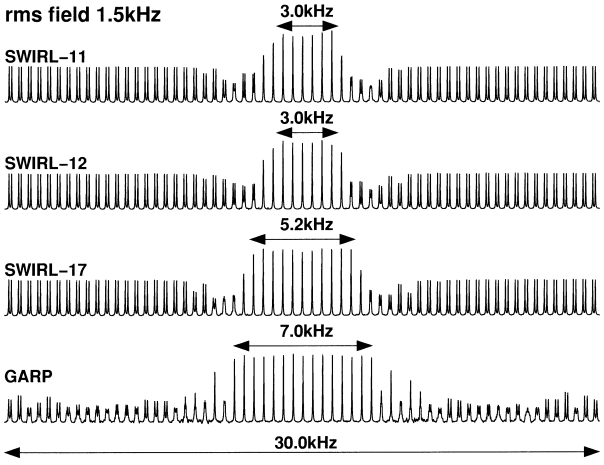

FIG. 3. (Upper three traces) Experimental decoupling profiles of the amplitude-modulated decoupling pulses SWIRL-11, SWIRL-12, and SWIRL-17. (Lowest trace) Decoupling profile for GARP. All four cases correspond to the same RF power level. The three SWIRLs are calibrated to give an RMS field of 1.50 kHz. The corresponding pulse durations and peak fields are $\tau = 3.92$ ms and $\omega_{peak}/2\pi = 3.41$ kHz for SWIRL-11, $\tau = 4.06$ ms and $\omega_{peak}/2\pi = 3.50$ kHz for SWIRL-12, and $\tau = 4.71$ ms and $\omega_{peak}/2\pi = 4.02$ kHz for SWIRL-17. The equivalent GARP sequence has a $\pi/2$ pulse duration of $\tau_{\pi/2} = 166.67$ μs and thus a constant decoupler field of $\omega_{GARP}/2\pi = 1.50$ kHz. Note that the SWIRL method gives broadband decoupling, yet resonances outside the operating band are unperturbed.

was performed for each waveform. The results are shown in Fig. 4. From these, it can be concluded that while the suppression of the sidebands is excellent in experiments for which the region to be decoupled is relatively wide, particularly narrowband applications of SWIRL decoupling at very low RMS fields may give rise to intolerable sideband excitation.

The final experimental test of the quality of the SWIRL decoupling scheme involved an assessment of the sensitivity to misadjustments of the magnitude of the RF field away from the values required for an optimal performance. From the results of this which are summarized in Fig. 5, it is clear that the modulations are highly robust with respect to even a 10% miscalibration and are thus expected to be equally tolerant to inhomogeneneities in the decoupler field.

As mentioned above, a knowledge of the normalized RMS and peak amplitudes Ω_{RMS} and Ω_{peak} of the SWIRL pulses (Tables 1 and 2) and the theoretical operating bandwidths (Figs. 1 and 2) is sufficient to predict the pulse durations τ and the actual peak RF amplitudes $\omega_{peak}/2\pi$ which are required to decouple over a particular range of resonance offsets. In the case of either SWIRL-11 or SWIRL-12 for which the operating range per unit RMS pulse amplitude is unity, it is clear that decoupling over a chosen frequency band which covers a resonance offset range $\pm\varpi/2\pi = \pm F$ is obtained with an RMS pulse amplitude of $\omega_{RMS}/2\pi = F$. The corresponding peak pulse amplitude and pulse duration are then determined from the definitions $\omega_{peak}/\omega_\tau = \Omega_{peak}$, $\omega_{RMS}/\omega_\tau = \Omega_{RMS}$, and $\omega_\tau = 2\pi/\tau$ which indicate that $\omega_{peak} = (\Omega_{peak}/\Omega_{RMS})\omega_{RMS}$ and $\tau = 2\pi\Omega_{RMS}/\omega_{RMS}$ and hence that $\omega_{peak}/2\pi = (\Omega_{peak}/\Omega_{RMS})F$ and $\tau = \Omega_{RMS}/F$. The peak pulse amplitude is in turn related to the duration of a hard $\pi/2$ pulse $\tau_{\pi/2} = 0.25(2\pi/\omega_{peak})$ which is calibrated at that power level. From the values of Ω_{peak} and Ω_{RMS}, it can thus be deduced that for a correctly adjusted SWIRL-11 modulation,

$$\omega_{peak}/2\pi = 2.27F,\ \tau = 5.88/F,$$
$$\text{and } \tau_{\pi/2} = 0.110/F \quad \text{for } \varpi/2\pi = F \qquad [15]$$

while for SWIRL-12,

$$\omega_{peak}/2\pi = 2.33F,\ \tau = 6.09/F,$$
$$\text{and } \tau_{\pi/2} = 0.107/F \quad \text{for } \varpi/2\pi = F. \qquad [16]$$

Similarly, the values of the normalized peak and RMS pulse fields and the fact that the theoretical decoupling bandwidth of SWIRL-17 is 75% greater than the RMS pulse amplitude indicate that this modulation will decouple over an offset range $\varpi/2\pi = F$ when

$$\omega_{peak}/2\pi = 1.53F,\ \tau = 12.36/F,$$
$$\text{and } \tau_{\pi/2} = 0.163/F \quad \text{for } \varpi/2\pi = F. \qquad [17]$$

The actual RMS pulse amplitudes and the pulse durations implemented in the above experiments confirm the value of a theoretical precalibration which is thus recommended prior to empirical adjustments of the pulse parameters despite the evident insensitivity of the decoupling scheme to incorrect power levels.

It has been shown theoretically and experimentally that an inherently cyclic amplitude-modulated pulse offers a feasible alternative to a composite decoupling cycle comprising a train of inversion elements. The particular modulations presented here and referred to as the SWIRL waveforms are built from a compact series of Fourier components following the example of the BURP pulses (*21*). As a result, practical implementation of the SWIRL waveforms is similarly straightforward and the band-selective characteristics are preserved. The method is broadband with respect to the deposition of RF power and the suppression of cycling sideband excitation is highly satisfactory providing the decoupled frequency band is sufficiently wide. A high degree of tolerance to miscalibration of the pulse parameters is expected, and a similarly insensitivity to RF inhomogeneities is envisioned. Further research will be directed at the design of alternative modulations which are more complex than the simple RF amplitude variations investigated here with the aim of improving the decoupling bandwidth attainable per unit RF power. A similar approach to the problem of hetero-

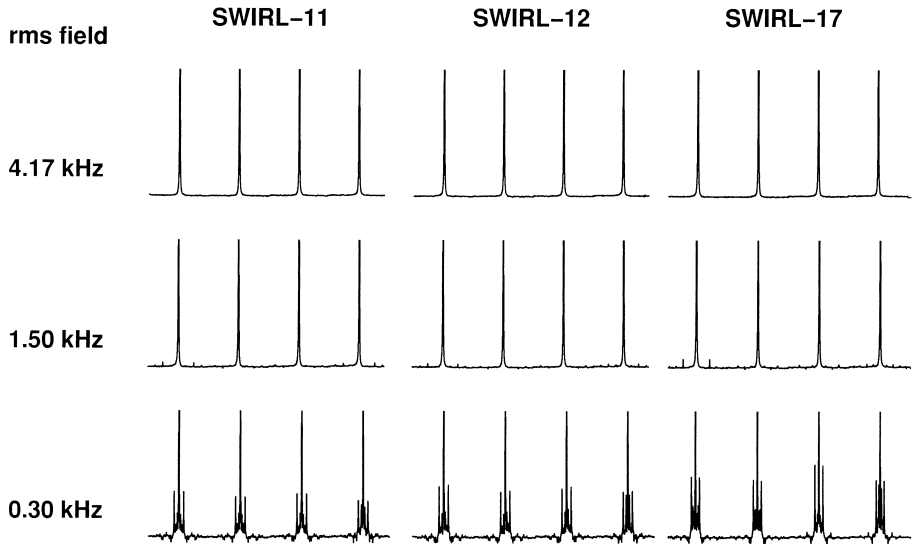

FIG. 4. Experimental measurement of the cycling sidebands excited by the SWIRL modulations. Three experiments are performed for each waveform using RMS pulse fields of 4.17 kHz (upper series), 1.50 kHz (central series), and 300 Hz (lower series). The series of four spectra representing each of the nine experiments correspond to four different values of the decoupler offset. Considering the spectra in order and from left to right, these frequencies are taken on the exact resonance, at one-third and then two-thirds of the way along the operating bandwidth, and finally at the bandwidth edge. The 4.17 kHz power level requires pulse durations and peak fields of $\tau = 1.41$ ms and $\omega_{peak}/2\pi = 9.46$ kHz for SWIRL-11, $\tau = 1.46$ ms and $\omega_{peak}/2\pi = 9.71$ kHz for SWIRL-12, and $\tau = 1.69$ ms and $\omega_{peak}/2\pi = 11.16$ kHz for SWIRL-17. The 1.50 kHz experiments use pulse durations and peak fields of $\tau = 3.92$ ms and $\omega_{peak}/2\pi = 3.41$ kHz for SWIRL-11, $\tau = 4.06$ ms and $\omega_{peak}/2\pi = 3.50$ kHz for SWIRL-12, and $\tau = 4.71$ ms and $\omega_{peak}/2\pi = 4.02$ kHz for SWIRL-17. The 300 Hz experiments use pulse durations and peak fields of $\tau = 19.60$ ms and $\omega_{peak}/2\pi = 0.68$ kHz for SWIRL-11, $\tau = 20.30$ ms and $\omega_{peak}/2\pi = 0.70$ kHz for SWIRL-12, and $\tau = 23.53$ ms and $\omega_{peak}/2\pi = 0.80$ kHz for SWIRL-17. Note the excellent level of sideband suppression at the high and intermediate power levels.

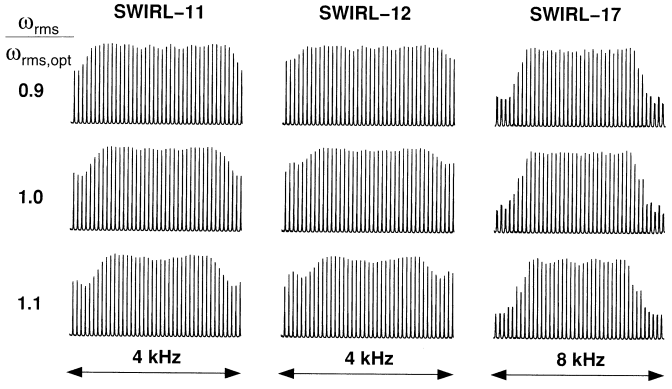

FIG. 5. Experimental evaluation of the tolerance of the SWIRL pulses to 10% missets in the RF field strength. Three experiments are shown for each waveform SWIRL-11 (left column), SWIRL-12 (central column), and SWIRL-17 (right column) which correspond to well-calibrated RMS fields (central series) and 10% missets below (upper series) and above (lower series) these levels. The correctly calibrated modulations have an RMS field of $\omega_{RMS,opt} = 1.50$ kHz, requiring pulse durations and peak fields of $\tau_{opt} = 3.92$ ms and $\omega_{peak,opt}/2\pi = 3.41$ kHz for SWIRL-11, $\tau_{opt} = 4.06$ ms and $\omega_{peak,opt}/2\pi = 3.50$ kHz for SWIRL-12, and $\tau_{opt} = 4.71$ ms and $\omega_{peak,opt}/2\pi = 4.02$ kHz for SWIRL-17. The misadjusted pulses differ from these only with respect to the amplitudes of the peak and hence the RMS pulse fields which are set at the erroneous values ω_{RMS} with no compensatory alterations to the pulse durations. Note the evident insensitivity of the waveforms to missets of this kind.

nuclear dipolar decoupling in solid-state MAS NMR is also under development.

ACKNOWLEDGMENTS

H.G. thanks Professor Beat Meier (Nijmegen) for allowing time on his computers to use a version of GAMMA adapted for Floquet simulations, and Marc Baldus (Nijmegen) and Sabine Hediger (Zurich) for their advice. H.G. is also grateful to the Royal Society for a University Research Fellowship.

REFERENCES

1. M. H. Levitt and R. Freeman, *J. Magn. Reson.* **43,** 502 (1981).
2. M. H. Levitt, R. Freeman, and T. Frenkiel, *J. Magn. Reson.* **47,** 328 (1982).
3. J. S. Waugh, *J. Magn. Reson.* **49,** 517 (1982).
4. J. S. Waugh, *J. Magn. Reson.* **50,** 30 (1982).
5. A. J. Shaka, J. Keeler, and R. Freeman, *J. Magn. Reson.* **53,** 313 (1983).
6. A. J. Shaka, P. B. Barker, and R. Freeman, *J. Magn. Reson.* **64,** 547 (1985).
7. A. J. Shaka and J. Keeler, *Prog. NMR Spectrosc.* **19,** 47 (1987).
8. T. Fujiwara, T. Anai, N. Kurihara, and K. Nagayama, *J. Magn. Reson. A* **104,** 103 (1993).
9. Z. Starčuk, Jr., K. Bartusek, and Z. Starčuk, *J. Magn. Reson. A* **107,** 24 (1994).
10. M. R. Bendall, *J. Magn. Reson. A* **112,** 126 (1995).

11. Ē. Kupče and R. Freeman, *J. Magn. Reson. A* **115,** 273 (1995).
12. R. Fu and G. Bodenhausen, *Chem. Phys. Lett.* **245,** 415 (1995).
13. Ē. Kupče and R. Freeman, *J. Magn. Reson. A* **117,** 246 (1995).
14. R. Fu and G. Bodenhausen, *J. Magn. Reson. A* **117,** 324 (1995).
15. M. H. Levitt and R. Freeman, *J. Magn. Reson.* **33,** 473 (1979).
16. M. A. McCoy and L. Mueller, *J. Am. Chem. Soc.* **114,** 2108 (1992).
17. U. Eggenberger, P. Schmidt, M. Sattler, S. J. Glaser, and C. Griesinger, *J. Magn. Reson.* **100,** 604 (1992).
18. M. A. McCoy and L. Mueller, *J. Magn. Reson. A* **101,** 122 (1993).
19. U. Eggenberger, P. Schmidt, M. Sattler, S. J. Glaser, and C. Griesinger, *J. Magn. Reson.* **100,** 604 (1992).
20. H. Geen, *J. Phys. B* **29,** 1699 (1996).
21. H. Geen and R. Freeman, *J. Magn. Reson.* **93,** 93 (1991).
22. J. H. Shirley, *Phys. Rev. B* **138,** 979 (1965).
23. S. Vega, E. T. Olejniczak, and R. G. Griffin, *J. Chem. Phys.* **80,** 4832 (1984).
24. G. Goelman, S. Vega, and D. B. Zax, *Phys. Rev. A* **39,** 5725 (1989).
25. D. B. Zax and S. Vega, *Phys. Rev. Lett.* **62,** 1840 (1989).
26. S. Hediger, B. H. Meier, and R. R. Ernst, *Chem. Phys. Lett.* **213,** 627 (1993).
27. S. Hediger, B. H. Meier, and R. R. Ernst, *J. Chem. Phys.* **102,** 4000 (1995).
28. H. Salwen, *Phys. Rev.* **99,** 1274 (1955).
29. S. A. Smith, T. O. Levante, B. H. Meier, and R. R. Ernst, *J. Magn. Reson. A* **106,** 75 (1994).